Distance and angular holonomic constraints in molecular simulations

David Dubbeldam,[1,a)] Gloria A. E. Oxford,[2] Rajamani Krishna,[1] Linda J. Broadbelt,[2] and Randall Q. Snurr[2]
[1]*Van't Hoff Institute for Molecular Sciences, University of Amsterdam, Nieuwe Achtergracht 166, Amsterdam, Noord-Holland 1018WV, The Netherlands*
[2]*Department of Chemical and Biological Engineering, Northwestern University, 2145 Sheridan Road, Evanston, Illinois 60208, USA*

(Received 17 February 2010; accepted 23 April 2010; published online 20 July 2010)

Finding the energy minima of systems with constraints is a challenging problem. We develop a minimization method based on the projection operator technique to enforce distance and angle constraints in minimization and reaction-path dynamics. The application of the projection operator alone does not maintain the constraints, i.e., they are slightly violated. Therefore, we use the SHAKE-methodology to enforce the constraints after each minimization step. We have extended θ -SHAKE for bend angles and introduce ϕ -SHAKE and χ -SHAKE to constrain dihedral and out-of-plane angles, respectively. Two case studies are presented: (1) A mode analysis of united-atom *n*-butane with various internal degrees of freedom kept frozen and (2) the minimization of chromene at a fixed approach toward the catalytic site of a (salen)Mn. The obtained information on energetics can be used to explain why specific enantioselectivity is observed. Previous minimization methods work for the free molecular case, but fail when molecules are tightly confined. © *2010 American Institute of Physics*. [doi:10.1063/1.3429610]

I. INTRODUCTION

There are three basic types of calculations performed with classical atomistic models: Monte Carlo (MC) simulations, molecular dynamics (MD) simulations, and energy minimizations [sometimes referred to as molecular mechanics (MM)]. MC simulations use stochastic methods to probe configuration space; MD simulations solve the Newton equations of motion; and energy minimizations find local and/or global energy minima for a molecular system. In many systems, we have to reckon with constraints. For example, it is common to use rigid bodies to describe small gas molecules in which the interatomic distances are fixed. Formally, we have to distinguish between holonomic and nonholonomic constraints.[1] Holonomic systems have constraints that can be expressed as an equation relating the particle coordinates of the type $f(\mathbf{r}_1,\mathbf{r}_1,\mathbf{r}_3,\ldots,t)=0$, where $\mathbf{r}_i$ is the vector of Cartesian coordinates of particles. A constraint that cannot be expressed in this form is a nonholonomic constraint. Common holonomic constraints are rigid bodies and fixed bond lengths and bend and dihedral angles.

In mechanics, a constraint algorithm is a method of satisfying constraints for bodies that obey Newton's equations of motion. The main difficulties are that the coordinates are not all independent and the forces of the constraints are not known in advance. There are three basic approaches to satisfying constraints: (1) Formulating the problem in terms of unconstrained internal or generalized coordinates, (2) introducing explicit constraint forces such as harmonic potentials, and (3) determining the coordinate adjustments necessary to satisfy the constraints, e.g., by the technique of Lagrangian multipliers. The first solution is to define new generalized coordinates that are unconstrained; this can be applied, for example, to keep small molecules rigid. Instead of constraining the intramolecular distances, one can redefine the problem in internal coordinates: The center of mass and elements of the rotation matrix.[2,3] The second approach is often termed "soft" constraints. Soft constraints can be viewed as additional energy penalty functions, usually harmonic in functional form. A serious disadvantage is that the force constants need to be sufficiently large to satisfy the constraints, leading to numerical problems. The third approach is to solve the "hard" constraints to determine the coordinate adjustments necessary to satisfy the constraints. In the Lagrangian approach of undetermined multipliers, one variable (the Lagrangian multiplier) is added to the system for each constraint. By determining the value of the Lagrangian multipliers one can then compute the forces induced by the constraints. In computer simulations, many algorithms focus on procedures to estimate Lagrangian multipliers numerically. It is possible to find the Lagrangian multipliers analytically in some cases.[4]

MC methods[5–7] are readily adapted to constraints. One simply uses MC moves that leave the constraints satisfied. For example, for rigid molecules, one uses translation and rotation of the molecule, which leaves the internal structure intact. In terms of the three ways of handling the constraints, one can say that MC is most suited to the first type of solu-

[a)]Electronic mail: d.dubbeldam@uva.nl.

tion, i.e., to define the MC move in terms of generalized coordinates. MC will not be discussed further and we will focus on MD and energy minimization.

Constraints are often incorporated in MD simulations. In MD simulations,[5–8] successive configurations of the system are generated by integrating Newton's laws of motion, which yields a trajectory that describes the positions, velocities, and accelerations of the particles as they vary with time. The numerical scheme is rendered difficult by the small time step required for the numerical integration of fast motions in the system. It is therefore common to treat selected degrees of freedom as rigid, e.g., methyl groups, water, and CO_2. Ryckaert *et al.*[9] used the Lagrangian multiplier approach to develop the SHAKE algorithm for applying bond-stretch constraints in MD. SHAKE is designed to be used in combination with the basic Verlet integration scheme. To avoid the computational drawbacks of the basic Verlet scheme, Andersen[10] used instead the velocity-Verlet algorithm and named the resulting algorithm RATTLE. To impose total rigidity of the water molecule, one can use triangulation (i.e., impose an additional length constraint on the H–H distance). However, a better approach is to use θ-SHAKE,[11] which allows for the explicit treatment of angular constraints. There are no physical reasons to restrict torsional or out-of-plane motion in MD. Constraining them can seriously alter the dynamics of the original, unconstrained system. Nevertheless, the ability to constrain dihedral angles can be useful in simulations in which one needs to assess the behavior of a molecule as a function of conformation.

In minimization and reaction-path dynamics,[7,12,13] it is useful to use such distance and angle constraints, for example, to study the approach of a molecule toward a catalytic site. Hard constraints in minimization can be solved by (1) a Lagrangian approach or (2) projection methods.[12,14] In the Lagrangian approach, one variable (the Lagrangian multiplier) is added to the system for each constraint, and one then searches for a stationary point in this extended system of equations. Projection methods involve the division of the search space into the null space and range space of the Jacobian of the constraints at each point of the search. The optimization then consists of minimization in the null space (i.e., parallel to the constraints). The target function to be optimized is still the original energy expression. The projection method is found to be superior in performance.[15] It is more stable and robust than Lagrangian methods and avoids the mixing of reaction coordinate and constraint modes that occurs easily in Lagrangian methods. The starting geometry and the geometry at every succeeding iteration must be "feasible," i.e., they must satisfy the constraints. Even if the starting configuration satisfies the constraints, the nonlinear character of the constraints means that the application of the projection operator will not maintain the feasibility of the iterates. Lu *et al.*[14] provided a method to maintain feasibility of the bond distance and bond angle constraints: For the bond distance, one of the atoms is displaced in the direction of the force until the constraint is satisfied, and to fulfill bond angle constraints, the two terminal atoms are displaced such that there are no changes in the bond distances.

In this work, we derive constraint expressions for use in SHAKE, RATTLE, energy minimization methods, and mode analysis. The remainder of this paper is organized as follows. We start with a brief introduction to the SHAKE methodology and the existing SHAKE methods for distance constraints and bend angle constraints. The latter is referred to in the literature as θ-SHAKE. We then introduce methods for constraining dihedral and out-of-plane angles, which we refer to as ϕ-SHAKE and χ-SHAKE, respectively. We also briefly discuss the RATTLE methodology in which the basic Verlet integration scheme is replaced by the velocity Verlet scheme. The SHAKE/RATTLE-constraint methodology can be used twofold: One can use these equations in MD, but here we specifically apply it to keep constraints satisfied during minimization. In Sec. IV, we describe the mode-following minimization and projection. The projection will not maintain the feasibility. We use an idea similar to Lu *et al.*[14] to restore it but replace their feasibility algorithm with more general SHAKE-type methods. SHAKE algorithms leave the center of mass and angular momentum unchanged. The method is reliable and flexible. Mode-following minimization methods use the first and second derivatives of the potentials. The latter, the Hessian matrix, is the central entity in mode analysis. The Hessian matrix is mass weighted, and we show how to project constraints such as bond, bend, dihedral, and out-of-plane angles from the mass-weighted Hessian matrix. We conclude with two case studies. We investigate united-atom *n*-butane with various constraints on the internal structure and compare the analytical solution of the frequencies to very low temperature MD simulation using RATTLE. The second case study concerns two real world examples: (a) The minimization of chromene at a fixed distance, bend angle, and dihedral angle toward a (salen)Mn catalyst and (b) the minimization of chromene at a fixed distance, bend angle, and dihedral angle toward a (salen)Mn strut in a periodic framework.

II. SHAKE METHODOLOGY

Before presenting our ϕ-SHAKE and χ-SHAKE method, we briefly introduce the SHAKE and θ-SHAKE methodology following the presentation of Gonnet *et al.*[11] The Verlet integration for time integration can be modified to enforce n_c constraints using Lagrange's method of undetermined multipliers,

$$\mathbf{r}_i^{(t+\Delta t)} = \tilde{\mathbf{r}}_i^{(t+\Delta t)} + \sum_{k=1}^{n_c} \lambda_k \mathbf{h}_{i,k}, \tag{1}$$

where

$$\mathbf{h}_{i,k} = \frac{\partial \sigma_k^{(t)}}{\partial \mathbf{r}_i^{(t)}} \frac{(\Delta t)^2}{m_i} \tag{2}$$

is the weighted constraint gradient of σ_k on $\mathbf{r}_i$, Δt is the integration time step, $\tilde{\mathbf{r}}_i^{(t+\Delta t)}$ is the unconstrained particle position at time $t+\Delta t$, m_i is the mass of atom i, and λ_k are the Lagrangian multipliers. The constraint equation for distance constraints between atom a and b is

$$\sigma_k^{(t)} = |\mathbf{r}_{k,a}^{(t)} - \mathbf{r}_{k,b}^{(t)}|^2 - d_k^2 = 0, \quad k = 1, \ldots, n_c \tag{3}$$

where d_k is the fixed bond distance of constraint k and $\mathbf{r}_{k,a}$ and $\mathbf{r}_{k,b}$ denote the positions of atoms a and b, associated with constraint k. Substitution of Eq. (1) into Eq. (3) leads to

$$\sigma_k^{(t)} = \left| \tilde{\mathbf{r}}_{k,a}^{(t)} + \sum_{l=1}^{n_c} \lambda_l \mathbf{h}_{ka,l} - \left(\tilde{\mathbf{r}}_{k,b}^{(t)} + \sum_{l=1}^{n_c} \lambda_l \mathbf{h}_{kb,l} \right) \right|^2 - d_k^2. \tag{4}$$

In SHAKE, the constraints are treated as decoupled,

$$\sigma_k^{(t)} = |\tilde{\mathbf{r}}_{k,a}^{(t)} + \lambda_k \mathbf{h}_{ka,k} - (\tilde{\mathbf{r}}_{k,b}^{(t)} + \lambda_k \mathbf{h}_{kb,k})|^2 - d_k^2. \tag{5}$$

The kth constraint equation for λ_k can be solved using Newton's method,

$$\lambda_k = - \left. \frac{\sigma_k}{\partial \sigma_k / \partial \lambda_k} \right|_{\lambda_{l=0}, l=1,\ldots,n_c}. \tag{6}$$

The general outline of the iterative SHAKE method is shown in Algorithm 1.

Algorithm 1: r^2 -SHAKE: $\sigma_k = r_{k,ab}^2 - d_k^2 = 0$

for $k = 1, \ldots, n_c$ **do**

$$\mathbf{h}_{k,a} = \frac{\partial \sigma_k^{(t)}}{\partial \mathbf{r}_{k,a}^{(t)}} \frac{(\Delta t)^2}{m_{k,a}} = 2(\mathbf{r}_{k,a}^{(t)} - \mathbf{r}_{k,b}^{(t)}) \frac{(\Delta t)^2}{m_{k,a}}$$

$$\mathbf{h}_{k,b} = \frac{\partial \sigma_k^{(t)}}{\partial \mathbf{r}_{k,b}^{(t)}} \frac{(\Delta t)^2}{m_{k,b}} = -2(\mathbf{r}_{k,a}^{(t)} - \mathbf{r}_{k,b}^{(t)}) \frac{(\Delta t)^2}{m_{k,b}}$$

end for

Repeat

for $k = 1, \ldots, n_c$ **do**

$$\lambda_k^{(s)} = - \left. \frac{\sigma_k}{\partial \sigma_k / \partial \lambda_k} \right|_{\lambda_{l=0}, l=1,\ldots,n_c} = \frac{|\mathbf{r}_{k,a}^{(s-1)} - \mathbf{r}_{k,b}^{(s-1)}|^2 - d_k^2}{2(\mathbf{r}_{k,a}^{(s-1)} - \mathbf{r}_{k,b}^{(s-1)}) \cdot (\mathbf{h}_{k,a} - \mathbf{h}_{k,b})}$$

$$\mathbf{r}_{k,a}^{(s)} \leftarrow \mathbf{r}_{k,a}^{(s-1)} - \lambda_k^{(s)} \mathbf{h}_{k,a}$$

$$\mathbf{r}_{k,b}^{(s)} \leftarrow \mathbf{r}_{k,b}^{(s-1)} - \lambda_k^{(s)} \mathbf{h}_{k,b}$$

end for

until $\max_k \frac{|\sigma_k^{(s)}|}{2d_k^2} < \epsilon$.

First, the weighted constraint gradients are computed. These are the constraint gradients *before* the integration step. After integrating the unconstrained equations of motion, all atoms involved in constraints are moved along the direction of these constraint gradients until the constraints are satisfied. This iterative process is denoted by the superscript (s) indicating the current step and $(s-1)$ indicating the result of the previous step. The procedure is terminated when the stopping criteria are satisfied, i.e., when constraints are sufficiently close to zero denoted by a relative tolerance ϵ on the order of $\epsilon \approx 10^{-6}$ or 10^{-7}. Because the constraints are satisfied at the initial configuration and the solution of the previous integration step is in the vicinity of the current solution, one can safely use Newton's method to solve for the fixed point. In principle, Newton's method has quadratic convergence. However, since the constraints are treated as if they were independent, the algorithm converges linearly, i.e., despite the fact that updating one constraint slightly degrades the results already obtained for the other constraints, convergence is achieved.[16] Many variants of SHAKE are proposed, among them are SETTLE,[17] GRADIENT SHAKE,[18] NIMM,[19] LINCS,[20] QSHAKE,[21] GSHAKE,[22] GNIMM,[23] M-SHAKE,[24] WIGGLE,[25] P-SHAKE,[26] P-LINCS,[27] MILC-SHAKE,[28] θ -SHAKE,[11] and MILCH-SHAKE.[29] These algorithms differ mostly in the tradeoff between convergence and computational cost and in applicability to, e.g., linear and/or cyclic molecules. Note that the conventional SHAKE algorithm for bond distances uses r^2. In the Supplementary Material, we also have listed the r -SHAKE expressions.[30] This shows that the r^2-form is slightly more convenient and computationally less expensive.

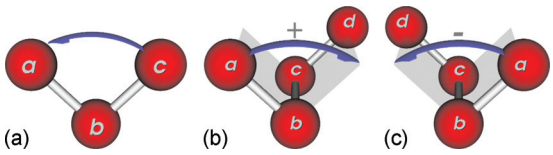

FIG. 1. The bend angle θ (a) defined by the angle formed by atoms a-b-c and the dihedral angle ϕ defined by the angle between the planes formed by atoms a-b-c and b-c-d. A positive dihedral angle (b) and a negative dihedral angle (c) are shown.

Before discussion of SHAKE for angles, the symbols used in the mathematical expressions are described. Let $\cdot$ denote the dot product, $\times$ denote the crossproduct, and $\mathbf{r}_{k,a}$, $\mathbf{r}_{k,b}$, $\mathbf{r}_{k,c}$, and $\mathbf{r}_{k,d}$ denote the positions of atoms a, b, c, and d, respectively, associated with constraint k. For notational convenience, we will drop the subscript k, where it is implicitly understood that the constraints should be solved iteratively according to Algorithm 1. Let the vector directed from atom a toward atom b be denoted by $\mathbf{r}_{ab} = \mathbf{r}_b - \mathbf{r}_a$, $\hat{\mathbf{r}}_{ab} = \mathbf{r}_{ab}/r_{ab}$ denotes the unit vector, $r_{ab} = |\mathbf{r}_{ab}| = \sqrt{\mathbf{r}_{ab} \cdot \mathbf{r}_{ab}}$, and $\mathbf{h}_{ab} = \mathbf{h}_b - \mathbf{h}_a$. To develop the algorithms to keep bend angles, torsion angles, and out-of-plane angles fixed, one can apply the same methodology as Algorithm 1. We will need expressions for the constraint gradients $\mathbf{h}$ and the constraint gradient $\partial \sigma_k / \partial \lambda_k$.

Gonnet *et al.*[11] developed the θ -SHAKE algorithm, which we here will name $\cos^2\theta$ -SHAKE because it is defined in terms of $\cos^2\theta$. The bend angle between atoms a, b, and c (Fig. 1) is defined as

$$\theta = \cos^{-1}\left(\frac{\mathbf{r}_{ba}\cdot\mathbf{r}_{bc}}{r_{ba}r_{bc}}\right). \tag{7}$$

The constraint for angles can be defined in various ways, e.g.,

$$\sigma = \cos^2\,\theta_{abc} - \cos^2\,\theta_0 = 0, \tag{8}$$

where θ_0 is the fixed bend angle. To obtain the constraint gradient $\partial\sigma_k/\partial\lambda_k$, Gonnet *et al.*[26] substituted $\mathbf{r}_{ba}=\mathbf{r}_{ba}+\lambda\mathbf{h}_{ba}$ and $\mathbf{r}_{bc}=\mathbf{r}_{bc}+\lambda\mathbf{h}_{bc}$ into Eqs. (7) and (8), took the derivative with respect to λ, and subsequently set $\lambda=0$ because the particle positions are updated in each step and the multipliers are therefore reset to their original values of zero. This is called linearization in Ryckaert *et al.*[9] and eliminates all terms linear in λ_l in σ_k and all terms quadratic in λ_l in both σ_k and $\partial\sigma_k/\partial\lambda_k$.[26] The result after setting $\lambda=0$ is

$$\frac{\partial\sigma_k}{\partial\lambda_k} = 2\,\cos\,\theta\left[\frac{(\mathbf{r}_{ba}\cdot\mathbf{h}_{bc})+(\mathbf{r}_{bc}\cdot\mathbf{h}_{ba})}{r_{ba}r_{bc}} - \left(\frac{(\mathbf{r}_{ba}\cdot\mathbf{h}_{ba})}{r_{ba}^2}+\frac{(\mathbf{r}_{bc}\cdot\mathbf{h}_{bc})}{r_{bc}^2}\right)\cos\,\theta\right] \tag{9}$$

and the Cartesian derivatives of $\cos^2\,\theta$ are

$$\nabla\,\cos^2\,\theta_{abc}(a) = -\,2\,\cos\,\theta\frac{\cos\,\theta\hat{\mathbf{r}}_{ba}-\hat{\mathbf{r}}_{bc}}{r_{ba}}, \tag{10}$$

$$\nabla\,\cos^2\,\theta_{abc}(b) = -\,(\nabla\,\cos^2\,\theta_{abc}(a)+\nabla\,\cos^2\,\theta_{abc}(c)), \tag{11}$$

$$\nabla\,\cos^2\,\theta_{abc}(c) = -\,2\,\cos\,\theta\frac{\cos\,\theta\hat{\mathbf{r}}_{bc}-\hat{\mathbf{r}}_{ba}}{r_{bc}}. \tag{12}$$

Of course, the constraint for angles can be defined in other ways,

$$\sigma = \theta_{abc} - \theta_0 = 0, \tag{13}$$

$$\sigma = \cos\,\theta_{abc} - \cos\,\theta_0 = 0. \tag{14}$$

The first constraint type [Eq. (13)] is here named θ -SHAKE. The gradient of θ_{abc} in Cartesian coordinates is the Wilson vector for valence angle bending,[31]

$$\nabla\theta(a) = \frac{\cos\,\theta\hat{\mathbf{r}}_{ba}-\hat{\mathbf{r}}_{bc}}{r_{ba}\,\sin\,\theta}, \tag{15}$$

$$\nabla\theta(b) = -\,(\nabla\theta_{abc}(a)+\nabla\theta_{abc}(c)), \tag{16}$$

$$\nabla\theta(c) = \frac{\cos\,\theta\hat{\mathbf{r}}_{bc}-\hat{\mathbf{r}}_{ba}}{r_{bc}\,\sin\,\theta}, \tag{17}$$

$$\frac{\partial\sigma_k}{\partial\lambda_k} = \frac{1}{\sin\,\theta}\left[\left(\frac{(\mathbf{r}_{ba}\cdot\mathbf{h}_{ba})}{r_{ba}^2}+\frac{(\mathbf{r}_{bc}\cdot\mathbf{h}_{bc})}{r_{bc}^2}\right)\cos\,\theta - \frac{(\mathbf{r}_{ba}\cdot\mathbf{h}_{bc})+(\mathbf{r}_{bc}\cdot\mathbf{h}_{ba})}{r_{ba}r_{bc}}\right]. \tag{18}$$

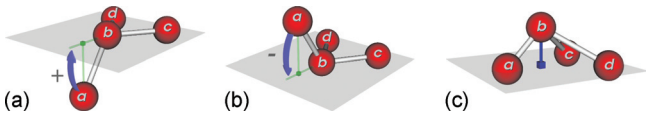

FIG. 2. The definition of the Wilson-type out-of-plane bend angle χ. A positive Wilson angle (a) and a negative Wilson angle (b) are shown along with an alternative definition using the out-of-plane distance (c).

To avoid the division by $\sin\,\theta$, which can cause numerical problems when $\theta\rightarrow 180°$, one can instead use the gradient of $\cos\,\theta$, an algorithm which we denote $\cos\,\theta$ -SHAKE,

$$\nabla\,\cos\,\theta(a) = -\,\frac{\cos\,\theta\hat{\mathbf{r}}_{ba}-\hat{\mathbf{r}}_{bc}}{r_{ba}}, \tag{19}$$

$$\nabla\,\cos\,\theta(b) = -\,(\nabla\,\cos\,\theta_{abc}(a)+\nabla\,\cos\,\theta_{abc}(c)), \tag{20}$$

$$\nabla\,\cos\,\theta(c) = -\,\frac{\cos\,\theta\hat{\mathbf{r}}_{bc}-\hat{\mathbf{r}}_{ba}}{r_{bc}}, \tag{21}$$

$$\frac{\partial\sigma_l}{\partial\lambda_l} = \frac{(\mathbf{r}_{ba}\cdot\mathbf{h}_{bc})+(\mathbf{r}_{bc}\cdot\mathbf{h}_{ba})}{r_{ba}r_{bc}} - \left(\frac{(\mathbf{r}_{ba}\cdot\mathbf{h}_{ba})}{r_{ba}^2}+\frac{(\mathbf{r}_{bc}\cdot\mathbf{h}_{bc})}{r_{bc}^2}\right)\cos\,\theta. \tag{22}$$

The relation between θ -SHAKE, $\cos\,\theta$ -SHAKE, and $\cos^2\,\theta$ -SHAKE is given by simple chain rules,

$$\frac{\mathrm{d}\,\cos(f(x))}{\mathrm{d}x} = -\,\sin\,(f(x))\frac{\mathrm{d}f(x)}{\mathrm{d}x}, \tag{23}$$

$$\frac{\mathrm{d}\,\cos^2(f(x))}{\mathrm{d}x} = -\,2\,\cos(f(x))\sin(f(x))\frac{\mathrm{d}f(x)}{\mathrm{d}x}. \tag{24}$$

In this work, we follow the procedure of Gonnet *et al.*[11] to derive the equations for dihedral angles (Fig. 1) and Wilson-type out-of-plane bending angles (Fig. 2). The dihedral angle between atoms $\mathbf{r}_a$, $\mathbf{r}_b$, $\mathbf{r}_c$, and $\mathbf{r}_d$ is given by

$$\phi = \cos^{-1}\left(\frac{(\mathbf{r}_{ab}\times\mathbf{r}_{bc})\cdot(\mathbf{r}_{bc}\times\mathbf{r}_{cd})}{|\mathbf{r}_{ab}\times\mathbf{r}_{bc}||\mathbf{r}_{bc}\times\mathbf{r}_{cd}|}\right) = \frac{(\mathbf{r}_{ab}\times\mathbf{r}_{bc})\cdot(\mathbf{r}_{bc}\times\mathbf{r}_{cd})}{\sin\,\theta_{abc}\,\sin\,\theta_{bcd}}. \tag{25}$$

We write the constraint equation as

$$\sigma = \phi - \phi_0. \tag{26}$$

Note that, unlike the bend angle, the sign of the torsion angle is important. A constraint equation using $\cos\,\phi$ does not discriminate between $-\phi$ and $+\phi$. This could lead to difficulties when constraining the dihedral angle to a value close to zero.

The gradient of ϕ_{abcd} in Cartesian coordinates is the Wilson vector for torsion,[31]

$$\nabla\phi(a) = -\frac{\hat{\mathbf{r}}_{ab}\times\hat{\mathbf{r}}_{bc}}{r_{ab}\sin^2\theta_{abc}}, \tag{27}$$

$$\nabla\phi(b) = \frac{r_{bc}-r_{ab}\cos\phi_{abc}}{r_{bc}r_{ab}\sin\phi_{abc}}\frac{\hat{\mathbf{r}}_{ab}\times\hat{\mathbf{r}}_{bc}}{\sin\phi_{abc}} + \frac{\cos\theta_{bcd}}{r_{bc}\sin\theta_{bcd}}\frac{\hat{\mathbf{r}}_{dc}\times\hat{\mathbf{r}}_{cb}}{\sin\theta_{bcd}}, \tag{28}$$

$$\nabla\phi(c) = \frac{r_{bc}-r_{dc}\cos\phi_{bcd}}{r_{bc}r_{dc}\sin\phi_{bcd}}\frac{\hat{\mathbf{r}}_{dc}\times\hat{\mathbf{r}}_{cb}}{\sin\phi_{bcd}} + \frac{\cos\theta_{abc}}{r_{bc}\sin\theta_{abc}}\frac{\hat{\mathbf{r}}_{ab}\times\hat{\mathbf{r}}_{bc}}{\sin\theta_{abc}}, \tag{29}$$

$$\nabla\phi(d) = -\frac{\hat{\mathbf{r}}_{dc}\times\hat{\mathbf{r}}_{cb}}{r_{dc}\sin^2\theta_{bcd}}. \tag{30}$$

We substitute $\mathbf{r}_{ab}=\mathbf{r}_{ab}+\lambda\mathbf{h}_{ab}$, $\mathbf{r}_{bc}=\mathbf{r}_{bc}+\lambda\mathbf{h}_{bc}$, and $\mathbf{r}_{dc}=\mathbf{r}_{dc}+\lambda\mathbf{h}_{dc}$ into Eqs. (25) and (26), take the derivative with respect to λ, and subsequently set $\lambda=0$. After some tedious algebra, we arrive at the ϕ -SHAKE expression for the dihedral angle case,

$$\frac{d\sigma}{d\lambda} = \frac{1}{\sin\phi}\left\{\frac{(\mathbf{r}_{ab}\times\mathbf{r}_{bc})\cdot(\mathbf{r}_{cd}\times\mathbf{h}_{bc}+\mathbf{h}_{cd}\times\mathbf{r}_{bc})+(\mathbf{r}_{bc}\times\mathbf{r}_{cd})\cdot(\mathbf{r}_{bc}\times\mathbf{h}_{ab}+\mathbf{h}_{bc}\times\mathbf{r}_{ab})}{|\mathbf{r}_{ab}\times\mathbf{r}_{bc}||\mathbf{r}_{bc}\times\mathbf{r}_{cd}|} - \left[\frac{(\mathbf{r}_{ab}\times\mathbf{r}_{bc})\cdot(\mathbf{r}_{bc}\times\mathbf{h}_{ab}+\mathbf{h}_{bc}\times\mathbf{r}_{ab})}{|\mathbf{r}_{ab}\times\mathbf{r}_{bc}|^2}+\frac{(\mathbf{r}_{bc}\times\mathbf{r}_{cd})\cdot(\mathbf{r}_{cd}\times\mathbf{h}_{bc}+\mathbf{h}_{cd}\times\mathbf{r}_{bc})}{|\mathbf{r}_{bc}\times\mathbf{r}_{cd}|^2}\right]\cos\phi\right\}. \tag{31}$$

We name the algorithm ϕ -SHAKE. Alternatives are $\sigma=\cos\phi-\cos\phi_0$ ($\cos\phi$ -SHAKE) and $\sigma=\cos^2\phi-\cos^2\phi_0$ ($\cos^2\phi$ -SHAKE). The expressions are easily derived by using Eqs. (23) and (24) and are given in the Supplementary Material as Algorithms S9 and S10, respectively.[30]

Finally, the Wilson angle (also called "wag"-angle or "inversion bend") is addressed. This angle involves an atom b bonded to atoms a, c, and d and is the angle between one of the bonds and the plane defined by the other two bonds. The angle is not uniquely defined and depends on the order of the atoms,

$$\chi^a = \sin^{-1}\left(\frac{\hat{\mathbf{r}}_{bd}\times\hat{\mathbf{r}}_{bc}}{\sin\theta_{cbd}}\cdot\hat{\mathbf{r}}_{ba}\right), \tag{32}$$

$$\chi^c = \sin^{-1}\left(\frac{\hat{\mathbf{r}}_{ba}\times\hat{\mathbf{r}}_{bd}}{\sin\theta_{abd}}\cdot\hat{\mathbf{r}}_{bc}\right), \tag{33}$$

$$\chi^d = \sin^{-1}\left(\frac{\hat{\mathbf{r}}_{bc}\times\hat{\mathbf{r}}_{ba}}{\sin\theta_{abc}}\cdot\hat{\mathbf{r}}_{bd}\right). \tag{34}$$

It is therefore customary to use the averaged Wilson angle,

$$\chi = \frac{\chi^a+\chi^c+\chi^d}{3}. \tag{35}$$

The Wilson angle constraint is

$$\sigma = \chi-\chi_0. \tag{36}$$

The gradients at the positions of atoms a, b, c, and d are given by

$$\nabla\chi(a) = \frac{1}{3r_{ba}}\left(\frac{\hat{\mathbf{r}}_{bd}\times\hat{\mathbf{r}}_{bc}}{\cos\chi^a\sin\theta_{cbd}}-\hat{\mathbf{r}}_{ba}\tan\chi^a\right) + \frac{1}{3r_{ba}}\left[\frac{\hat{\mathbf{r}}_{bd}\times\hat{\mathbf{r}}_{bc}}{\cos\chi^d\sin\theta_{abc}}-\frac{\tan\chi^d}{\sin^2\theta_{abc}}(\hat{\mathbf{r}}_{ba}-\hat{\mathbf{r}}_{bc}\cos\theta_{abc})\right]+\frac{1}{3r_{ba}}\left[\frac{\hat{\mathbf{r}}_{bd}\times\hat{\mathbf{r}}_{bc}}{\cos\chi^c\sin\theta_{abd}}-\frac{\tan\chi^c}{\sin^2\theta_{abd}}(\hat{\mathbf{r}}_{ba}-\hat{\mathbf{r}}_{bd}\cos\theta_{abd})\right], \tag{37}$$

$$\nabla\chi(c) = \frac{1}{3r_{bc}}\left(\frac{\hat{\mathbf{r}}_{ba}\times\hat{\mathbf{r}}_{bd}}{\cos\chi^c\sin\theta_{abd}}-\hat{\mathbf{r}}_{bc}\tan\chi^c\right) + \frac{1}{3r_{bc}}\left[\frac{\hat{\mathbf{r}}_{ba}\times\hat{\mathbf{r}}_{bd}}{\cos\chi^a\sin\theta_{cbd}}-\frac{\tan\chi^a}{\sin^2\theta_{cbd}}(\hat{\mathbf{r}}_{bc}-\hat{\mathbf{r}}_{bd}\cos\theta_{cbd})\right]+\frac{1}{3r_{bc}}\left[\frac{\hat{\mathbf{r}}_{ba}\times\hat{\mathbf{r}}_{bd}}{\cos\chi^d\sin\theta_{abc}}\right.$$

$$-\frac{\tan\chi^d}{\sin^2\theta_{abc}}(\hat{\mathbf{r}}_{bc}-\hat{\mathbf{r}}_{ba}\cos\theta_{abc})\Bigg], \tag{38}$$

$$\nabla\chi(d)=\frac{1}{3r_{bd}}\left(\frac{\hat{\mathbf{r}}_{bc}\times\hat{\mathbf{r}}_{ba}}{\cos\chi^d\sin\theta_{abc}}-\hat{\mathbf{r}}_{bd}\tan\chi^d\right)+\frac{1}{3r_{bd}}\left[\frac{\hat{\mathbf{r}}_{bc}\times\hat{\mathbf{r}}_{ba}}{\cos\chi^c\sin\theta_{abd}}-\frac{\tan\chi^c}{\sin^2\theta_{abd}}(\hat{\mathbf{r}}_{bd}-\hat{\mathbf{r}}_{ba}\cos\theta_{abd})\right]+\frac{1}{3r_{bd}}\left[\frac{\hat{\mathbf{r}}_{bc}\times\hat{\mathbf{r}}_{ba}}{\cos\chi^a\sin\theta_{cbd}}-\frac{\tan\chi^a}{\sin^2\theta_{cbd}}(\hat{\mathbf{r}}_{bd}-\hat{\mathbf{r}}_{bc}\cos\theta_{cbd})\right], \tag{39}$$

$$\nabla\chi(b)=-(\nabla\chi(a)+\nabla\chi(c)+\nabla\chi(d)). \tag{40}$$

We substitute $\mathbf{r}_{ba}=\mathbf{r}_{ba}+\lambda\mathbf{h}_{ba}$, $\mathbf{r}_{bc}=\mathbf{r}_{bc}+\lambda\mathbf{h}_{bc}$, and $\mathbf{r}_{bd}=\mathbf{r}_{bd}+\lambda\mathbf{h}_{bd}$ into Eqs. (32)–(36), take the derivative with respect to λ, and subsequently set $\lambda=0$. Again, after some tedious algebra, we arrive at the χ -SHAKE expression for the Wilson angle,

$$\begin{aligned}\frac{d\sigma}{d\lambda}=\frac{1}{3}\Bigg\{&\frac{1}{\cos\chi^a}\left(\frac{\mathbf{h}_{ba}\cdot(\mathbf{r}_{bc}\times\mathbf{r}_{bd})+\mathbf{r}_{ba}\cdot(\mathbf{r}_{bd}\times\mathbf{h}_{bc}+\mathbf{h}_{bd}\times\mathbf{r}_{bc})}{r_{ba}r_{bc}r_{bd}\sin\theta_{cbd}}\right)\\&-\tan\chi^a\left[\frac{\mathbf{r}_{ba}\cdot\mathbf{h}_{ba}}{r_{ba}^2}+\frac{\mathbf{r}_{bc}\cdot\mathbf{h}_{bc}}{r_{bc}^2}+\frac{\mathbf{r}_{bd}\cdot\mathbf{h}_{bd}}{r_{bd}^2}+\frac{\cos^2\theta_{cbd}}{\sin^2\theta_{cbd}}\left(\frac{\mathbf{r}_{bc}\cdot\mathbf{h}_{bc}}{r_{bc}^2}+\frac{\mathbf{r}_{bd}\cdot\mathbf{h}_{bd}}{r_{bd}^2}\right)-\frac{\cos\theta_{cbd}}{\sin^2\theta_{cbd}}\left(\frac{\mathbf{r}_{bd}\cdot\mathbf{h}_{bc}+\mathbf{r}_{bc}\cdot\mathbf{h}_{bd}}{r_{bc}r_{bd}}\right)\right]\\&+\frac{1}{\cos\chi^c}\left(\frac{\mathbf{h}_{bc}\cdot(\mathbf{r}_{bd}\times\mathbf{r}_{ba})+\mathbf{r}_{bc}\cdot(\mathbf{r}_{ba}\times\mathbf{h}_{bd}+\mathbf{h}_{ba}\times\mathbf{r}_{bd})}{r_{ba}r_{bc}r_{bd}\sin\theta_{abd}}\right)\\&-\tan\chi^c\left[\frac{\mathbf{r}_{bc}\cdot\mathbf{h}_{bc}}{r_{bc}^2}+\frac{\mathbf{r}_{bd}\cdot\mathbf{h}_{bd}}{r_{bd}^2}+\frac{\mathbf{r}_{ba}\cdot\mathbf{h}_{ba}}{r_{ba}^2}+\frac{\cos^2\theta_{abd}}{\sin^2\theta_{abd}}\left(\frac{\mathbf{r}_{bd}\cdot\mathbf{h}_{bd}}{r_{bd}^2}+\frac{\mathbf{r}_{ba}\cdot\mathbf{h}_{ba}}{r_{ba}^2}\right)-\frac{\cos\theta_{abd}}{\sin^2\theta_{abd}}\left(\frac{\mathbf{r}_{ba}\cdot\mathbf{h}_{bd}+\mathbf{r}_{bd}\cdot\mathbf{h}_{ba}}{r_{bd}r_{ba}}\right)\right]\\&+\frac{1}{\cos\chi^d}\left(\frac{\mathbf{h}_{bd}\cdot(\mathbf{r}_{ba}\times\mathbf{r}_{bc})+\mathbf{r}_{bd}\cdot(\mathbf{r}_{bc}\times\mathbf{h}_{ba}+\mathbf{h}_{bc}\times\mathbf{r}_{ba})}{r_{ba}r_{bc}r_{bd}\sin\theta_{abc}}\right)\\&-\tan\chi^d\left[\frac{\mathbf{r}_{bd}\cdot\mathbf{h}_{bd}}{r_{bd}^2}+\frac{\mathbf{r}_{ba}\cdot\mathbf{h}_{ba}}{r_{ba}^2}+\frac{\mathbf{r}_{bc}\cdot\mathbf{h}_{bc}}{r_{bc}^2}+\frac{\cos^2\theta_{abc}}{\sin^2\theta_{abc}}\left(\frac{\mathbf{r}_{ba}\cdot\mathbf{h}_{ba}}{r_{ba}^2}+\frac{\mathbf{r}_{bc}\cdot\mathbf{h}_{bc}}{r_{bc}^2}\right)-\frac{\cos\theta_{abc}}{\sin^2\theta_{abc}}\left(\frac{\mathbf{r}_{bc}\cdot\mathbf{h}_{ba}+\mathbf{r}_{ba}\cdot\mathbf{h}_{bc}}{r_{ba}r_{bc}}\right)\right]\Bigg\}.\end{aligned} \tag{41}$$

The expressions for $\sin\chi$ -SHAKE ($\sigma=\sin\chi-\sin\chi_0$) and $\sin^2\chi$ -SHAKE ($\sigma=\sin^2\chi-\sin^2\chi_0$) follow from

$$\frac{\mathrm{d}\sin(f(x))}{\mathrm{d}x}=\cos(f(x))\frac{\mathrm{d}f(x)}{\mathrm{d}x}, \tag{42}$$

$$\frac{\mathrm{d}\sin^2(f(x))}{\mathrm{d}x}=2\cos(f(x))\sin(f(x))\frac{\mathrm{d}f(x)}{\mathrm{d}x} \tag{43}$$

and are given in the Supplementary Material as Algorithms S12 and S13, respectively.[30] All versions discriminate between $-\chi$ and χ, even close to 0°, but for structures close to $\chi_0=90°$, χ -SHAKE could be preferable.

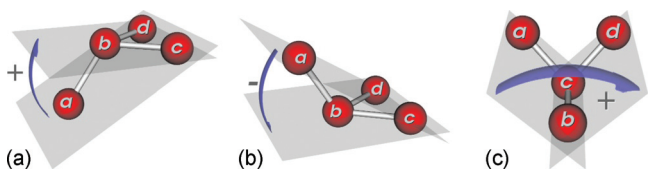

FIG. 3. A common definition of the improper dihedral angle ϕ: The angle between the planes formed by atoms "a-c-d" and "c-d-b." (a) A positive improper dihedral angle. (b) A negative improper dihedral angle. Note that an exchange of atoms "c" and "d" leads to a change in sign, but *not* in magnitude. (c) A second definition of the improper dihedral angle. Here, an exchange of terminal atoms "b" and "d" leads to a change in magnitude.

The improper torsion is an alternative for the out-of-plane angle (Fig. 3). Improper torsions are often used to keep sp^2 atoms planar and sp^3 atoms in a tetrahedral geometry. It is termed "improper torsion" because it simply treats the four atoms as if they were bonded in the same way as in a true torsional angle. Note that there are several definitions in use. A possible definition is to define the dihedral in terms of the angle between the planes *a-c-d* and *b-c-d*. A second definition uses *c* as the central atom and uses the planes between *a-b-c* and *b-c-d*. For improper torsions, an exchange of terminal atoms leads to a change in magnitude and/or sign of the angle, and the improper torsion needs to be symmetrized by adding additional improper torsions and rescaling the force constant (as done for the Wilson angle definition). Apart from these issues, the SHAKE expressions for improper dihedrals are identical to those for regular dihedrals.

III. CONSTRAINTS IN MD

Ryckaert *et al.*[9] introduced the "method of undetermined parameters" to ensure that the constraints are satisfied at each time step without introducing an additional numerical error

in the trajectory. The resulting SHAKE algorithm was introduced for bond constraints in combination with the Verlet integration scheme and later generalized to handle general forms of holonomic constraints.[32] To overcome the shortcomings of the basic Verlet algorithm, Andersen developed the velocity-Verlet version of SHAKE, named RATTLE.[10] Unlike the basic Verlet scheme, the velocity Verlet scheme updates both the positions and the velocities at each time step and therefore involves two stages [see Supplementary Material Algorithm S14 (Ref. 30)]. For general constraints, the two stages of the velocity Verlet algorithm are modified to satisfy the constraints as shown below.[16,33]

- Iteratively modify the positions $\mathbf{r}_i$ after stage 1,

$$\mathbf{r}_i^{(s)} = \mathbf{r}_i^{(s-1)} - \frac{(\Delta t)^2}{2}\frac{\gamma_k^{(s)}}{m_i}\nabla_i\sigma_k, \tag{44}$$

$$\gamma_k^{(s)} = \frac{2}{(\Delta t)^2}\frac{\sigma_k^{(s-1)}}{\Sigma_{i\in n_k}\frac{1}{m_i}(\nabla_i\sigma_k)^{(s-1)}\cdot\nabla_i\sigma_k}. \tag{45}$$

- Iteratively modify the velocities $\mathbf{v}_i$ after stage 2,

$$\mathbf{v}_i^{(s)} = \mathbf{v}_i^{(s-1)} - \frac{\Delta t}{2m_i}\delta_k^{(s)}\nabla_i\sigma_k, \tag{46}$$

$$\delta_k^{(s)} = \frac{2}{\Delta t}\frac{\Sigma_{i\in n_k}\mathbf{v}_i^{(s-1)}\cdot\nabla_i\sigma_k}{\Sigma_{i\in n_k}\frac{1}{m_i}|\nabla_i\sigma_k|^2}. \tag{47}$$

The Lagrangian multiplier $\lambda_k(t)$ can be estimated from

$$\lambda_k(t) \approx \sum \gamma_k^{(s)} \tag{48}$$

and is used to evaluate the stress and virial contribution.[16] Note that the velocity part has a different associated Lagrangian multiplier, and as a result, it is possible that both the positions and the velocities satisfy the constraints. The RATTLE algorithm is symplectic and time reversible when carried to convergence.[34]

The modification of the positions after stage 1 can alternatively be performed using SHAKE/Newton's method in a straightforward manner. It is also possible to perform both stages in a SHAKE-like fashion, e.g., a constraint procedure can be constructed for the velocity Verlet algorithm that requires only one evaluation of the constraint forces.[35]

IV. CONSTRAINTS IN MINIMIZATION

Efficient techniques have been developed for geometry optimization of a wide range of *ab initio* wave functions.[36] In self-consistent field calculations the wave function is gradually refined until consistency is achieved. Convergence is considerably improved by methods like direct inversion of the iterative subspace.[37] Constraints in quantum optimization are usually achieved by conversion to internal coordinates[38] or in Cartesian coordinates by Lagrangian multipliers and/or soft-constraints (penalty functions).[39,40] Fixed atoms can simply be eliminated from the optimization space when Cartesian coordinates are used. Likewise, using internal coordinate bond distances, bend and dihedral constraints can be eliminated from the optimization space. However, when using internal coordinates it is not obvious how to apply Cartesian constraints. Vice versa, imposing fixed bond distance, bend and dihedral angles are also not straightforward in Cartesian space because such constraints are complicated nonlinear functions of the Cartesian positions. However, projection methods can be used.[12,14,41] There are comparison studies between internal and Cartesian coordinates.[42] From a view point of flexibility, the Cartesian coordinates allow the most generic and versatile set of constraints. We use the exact Hessian and therefore Cartesian coordinates are expected to have similar convergence as internal coordinates.[43] Moreover, internal coordinates are more difficult to combine with structural periodicity.[44–46]

The most commonly applied minimization techniques for classical molecular systems are steepest descent (SD), conjugate gradient (CG), and Newton's methods.[47] The classical systems we focus on are periodic structures with hundreds to thousands of atoms. The resulting energy landscape is often complicated and jagged. In previous work[3] we found that methods such as CG, in principle, converge, but the solution was not a true minimum (it was a saddle point). The CG structure of the unit cell can be dramatically different from the (correct) zero Kelvin solution, e.g., for the IRMOF-1 metal-organic framework (MOF).[3]

Our aim is to develop a minimization technique applicable to adsorbates in tight periodic confinement where arbitrary constraints can be defined such as (a) fixed Cartesian positions, (b) fixed Cartesian distances between chosen pairs of atoms, (c) angle constraints between any three atoms, (d) dihedral constraints between any four atoms, and (e) out-of-plane constraints between any three atoms connected to a central atom. The algorithm is required to converge reliably and rapidly under the most difficult of numerical circumstances, and most importantly, we require that the obtained structure is a true minimum. Only the mode-following minimization technique can *guarantee* correct results. We combine this technique with constraints.

In this work, we focus on mode following, also known as Baker's minimization.[3,48] The method uses the gradients, the Hessian matrix, as well as the eigenvectors and eigenvalues of the Hessian matrix. The potential energy surface U of a (periodic) system can be Taylor expanded around a configuration $\mathbf{x}$ of the system,

$$U(\mathbf{x}+\delta\mathbf{x}) = U(\mathbf{x}) + \mathbf{g}^T\delta\mathbf{x} + \tfrac{1}{2}\delta\mathbf{x}^T\mathcal{H}\delta\mathbf{x} + \cdots, \tag{49}$$

where $\mathbf{g}=(\partial U/\partial x)$ is the gradient and $\mathcal{H}=\partial^2 U/\partial x_\alpha \partial x_\beta$ is referred to as the Hessian matrix. One can differentiate Eq. (49) with respect to $\delta\mathbf{x}$, set the result to zero, and solve to obtain what is known as the Newton–Raphson step,[49]

$$\delta\mathbf{x} = -\mathcal{H}^{-1}\mathbf{g}. \tag{50}$$

The Newton–Raphson step can also be expressed as a sum over the eigenvectors $\mathbf{A_i}$ (called local principle modes) and eigenvalues α_i of the Hessian matrix,

$$\delta\mathbf{x} = -\sum_i \frac{(\mathbf{A}_i^T\mathbf{g})}{\alpha_i}\mathbf{A}_i, \tag{51}$$

where $\mathbf{A}_i^T\mathbf{g}$ is the component of the gradient along the eigenmode $\mathbf{A}_i$. For zero eigenvalues, the corresponding step component is set to zero. A zero eigenvalue means that for a displacement in the direction of the eigenvector, the energy does not change, while positive and negative values mean an increase and decrease in energy, respectively. A true minimum has all positive eigenvalues, and a first order saddle point has exactly one negative eigenvalue. The Newton–Raphson steps minimize along the eigenvectors with positive eigenvalues and maximize along eigenvectors with negative eigenvalues. Therefore, when the starting configuration is of the correct curvature (the desired number of negative eigenvalues), the Newton–Raphson step is a good one to take.

In general, however, the step must be modified to obtain a structure of the desired curvature.[48] A simple but very powerful modification is to use a shift parameter γ, which shifts the value of the eigenvalues according to the following expression:[50]

$$\delta\mathbf{x} = -\sum_i \frac{\mathbf{A}_i^T\mathbf{g}}{\alpha_i-\gamma}\mathbf{A}_i. \tag{52}$$

Simons *et al.*[51] derived an equation to find the shift parameter γ,

$$\gamma = \sum_i \frac{(\mathbf{A}_i^T\mathbf{g})^2}{\gamma-\alpha_i}, \tag{53}$$

which can be solved by iteration. Note that besides minimization, the method can also be used to find saddle points.[48]

The set of $3N$ Cartesian coordinates is redundant. Only $3N-6$ coordinates are needed to describe the geometry of N atoms. It is important to prevent rotational and translational motions during minimization. The Eckart conditions provide a way of doing this. The full $3N\times 3N$ Hessian in Cartesian coordinates is treated by first projecting out vectors corresponding to translations and infinitesimal rotations constructed using[49]

$$\mathcal{T} = \begin{pmatrix} 1 & 0 & 0 \\ 0 & 1 & 0 \\ 0 & 0 & 1 \\ 1 & 0 & 0 \\ 0 & 1 & 0 \\ 0 & 0 & 1 \\ \vdots & \vdots & \vdots \\ 1 & 0 & 0 \\ 0 & 1 & 0 \\ 0 & 0 & 1 \end{pmatrix},$$

$$\mathcal{R} = \begin{pmatrix} 0 & z_1-c_z & -(y_1-c_y) \\ -(z_1-c_z) & 0 & x_1-c_x \\ y_1-c_y & -(x_1-c_x) & 0 \\ 0 & z_2-c_z & -(y_2-c_y) \\ -(z_2-c_z) & 0 & x_2-c_x \\ y_2-c_y & -(x_2-c_x) & 0 \\ \vdots & \vdots & \vdots \\ 0 & z_N-c_z & -(y_N-c_y) \\ -(z_N-c_z) & 0 & x_N-c_x \\ y_N-c_y & -(x_N-c_x) & 0 \end{pmatrix}, \tag{54}$$

where $\mathbf{c}=(1/N)\Sigma_i^N\mathbf{r}_i$ is the center of the system.

The translational constraints $\mathcal{T}$ and rotational constraints $\mathcal{R}$ form a set $\mathbf{e}_i, i=1\cdots 6$. The unit vectors $\mathbf{e}_i$ must be orthogonal to each other. A Gram–Schmidt orthogonalization can be carried out, and the vectors can be subsequently normalized. The orthogonal projector on the set $\mathbf{e}_i$ $(i=1,\ldots,m)$ can be written as

$$\mathcal{P} = \mathcal{I} - \sum_{i=1}^{m} \mathbf{e}_i(\mathbf{e}_i^T), \tag{55}$$

where $\mathcal{I}$ is the identity matrix. The matrix $\mathcal{P}$ of size $3N\times 3N$ can be used as a projection operator on first and second derivatives,

$$\mathbf{g}' = \mathcal{P}\mathbf{g}, \tag{56}$$

$$\mathcal{H}' = \mathcal{P}\mathcal{H}\mathcal{P}. \tag{57}$$

Lu and Truhlar[12,14] showed how to project out the bond distances and bend angles. The expressions given by Lu and Truhlar for bond distance and bend angles in Cartesian coordinates are the Cartesian gradients (Wilson vectors). Similarly, we use the same projection method for projecting out dihedral and out-of-plane angles. The set of projection vectors $\mathbf{e}_i$ is

$$\mathbf{e}^r = \frac{1}{N_r}\begin{pmatrix} 0 \\ \vdots \\ \nabla_x r_{ab}(a) \\ \nabla_y r_{ab}(a) \\ \nabla_z r_{ab}(a) \\ 0 \\ \vdots \\ \nabla_x r_{ab}(b) \\ \nabla_y r_{ab}(b) \\ \nabla_z r_{ab}(b) \\ 0 \\ \vdots \end{pmatrix}, \quad \mathbf{e}^\theta = \frac{1}{N_\theta}\begin{pmatrix} 0 \\ \vdots \\ \nabla_x \theta_{abc}(a) \\ \nabla_y \theta_{abc}(a) \\ \nabla_z \theta_{abc}(a) \\ 0 \\ \vdots \\ \nabla_x \theta_{abc}(b) \\ \nabla_y \theta_{abc}(b) \\ \nabla_z \theta_{abc}(b) \\ 0 \\ \vdots \\ \nabla_x \theta_{abc}(c) \\ \nabla_y \theta_{abc}(c) \\ \nabla_z \theta_{abc}(c) \\ 0 \\ \vdots \end{pmatrix}, \quad \mathbf{e}^\phi = \frac{1}{N_\phi}\begin{pmatrix} 0 \\ \vdots \\ \nabla_x \phi_{abcd}(a) \\ \nabla_y \phi_{abcd}(a) \\ \nabla_z \phi_{abcd}(a) \\ 0 \\ \vdots \\ \nabla_x \phi_{abcd}(b) \\ \nabla_y \phi_{abcd}(b) \\ \nabla_z \phi_{abcd}(b) \\ 0 \\ \vdots \\ \nabla_x \phi_{abcd}(c) \\ \nabla_y \phi_{abcd}(c) \\ \nabla_z \phi_{abcd}(c) \\ 0 \\ \vdots \\ \nabla_x \phi_{abcd}(d) \\ \nabla_y \phi_{abcd}(d) \\ \nabla_z \phi_{abcd}(d) \\ 0 \\ \vdots \end{pmatrix}, \quad \mathbf{e}^\chi = \frac{1}{N_\chi}\begin{pmatrix} 0 \\ \vdots \\ \nabla_x \chi_{abcd}(a) \\ \nabla_y \chi_{abcd}(a) \\ \nabla_z \chi_{abcd}(a) \\ 0 \\ \vdots \\ \nabla_x \chi_{abcd}(b) \\ \nabla_y \chi_{abcd}(b) \\ \nabla_z \chi_{abcd}(b) \\ 0 \\ \vdots \\ \nabla_x \chi_{abcd}(c) \\ \nabla_y \chi_{abcd}(c) \\ \nabla_z \chi_{abcd}(c) \\ 0 \\ \vdots \\ \nabla_x \chi_{abcd}(d) \\ \nabla_y \chi_{abcd}(d) \\ \nabla_z \chi_{abcd}(d) \\ 0 \\ \vdots \end{pmatrix}, \tag{58}$$

where N_r, N_θ, N_ϕ, and N_χ are normalization factors. Each vector in the set $\mathbf{e}_i$ corresponds to a particular constraint.

The outline of the minimization process is shown in Algorithm 2.

Algorithm 2: Mode-following minimization with constraints $\delta\mathbf{x}=0$

Repeat

$\mathbf{x} \rightarrow \mathbf{x}+\delta\mathbf{x}$

SHAKE all constraints

Compute energy, gradient, and Hessian

Project gradient and Hessian

Diagonalize Hessian to get eigenvalues and eigenvectors

Remove modes with zero eigenvalues from the optimization

Compute step vector $\delta\mathbf{x}$ from the shifted eigenvalues, the gradient,

and the eigenvectors

until every gradient $<\epsilon$ and all eigenvalues positive

Note that in our scheme it is allowed that the unit cell changes size and shape. In that case the state vector $\mathbf{x}$ contains in addition to the Cartesian coordinates of the atoms also six elements that represent the strain on the unit cell.[3,46]

One could also just project the gradients and use SD and/or CG. However, we have mentioned the downside of these methods. The projection of Lu and Truhlar was combined with a quasi-Newton method [Broyden-Fletcher-Goldfarb-Shanno (BGFS)].[14] Also here, the projected gradients are used (to construct the approximate projected inverse Hessian). For classical models the energy, gradients, and Hessian matrix are relatively cheap to compute, and we use the exact (projected) Hessian matrix (computed at each iteration).

Control of the step length is very important.[52] If the Hessian has small eigenvalues, the step may become very large and overshoot the minimum.[43] To achieve convergence we used a progressively smaller step length close to convergence based on the root mean square of the gradient,

$$\text{step length} = \min\left(0.3, \left[\frac{\Sigma_{i=1}^{n} g_i^2}{n}\right]^{\eta}\right), \tag{59}$$

where η is an convergence parameter. At each iteration, if the norm of $\delta\mathbf{x}$ is greater than the step length, then $\delta\mathbf{x}$ is scaled back to the step length. For optimization without constraints an η value of 0 (no scaling) works well. Common fixed step values are 0.3 for minimization and 0.1 for saddle-point searches. For most minimizations with constraints we used $\eta=1$, while for the hardest cases we encountered $\eta=1.2$ was sufficient. The downside of a higher η value is a slower convergence, but using this we were always able to lower the gradients on all atoms to values smaller than 10^{-6} kJ/mol Å while maintaining the constraints exactly (within a specified tolerance; in this work we used a relative

tolerance of 10^{-8}). Note that in our algorithm no line searches are necessary.

V. CONSTRAINTS AND NORMAL MODE ANALYSIS

Normal mode analysis (NMA) has become one of the standard techniques in the study of the dynamics of molecules. It is the study of motions of small amplitudes in harmonic potential wells by analytical means. Here, small means small enough that the harmonic approximation holds. Usually this means that harmonic vibrational analysis can provide a very good description of the system at low temperature. A NMA contains all time scales. However, disadvantages include limited motion around a single stable conformation and lack of anharmonic features that are small but sometimes important. Despite these obvious limitations, NMA has found widespread use.

The equation of motion of a molecule in a harmonic well is given by

$$\mathbf{M}\frac{d^2(\delta\mathbf{x})}{dt^2} = -\mathcal{H}\delta\mathbf{x}, \tag{60}$$

where $\mathbf{M}$ is a diagonal matrix that contains the masses of the atoms.[49,53] Substitution of the general solution $\delta\mathbf{x} = \mathbf{A}\cos(\omega t+\phi)$ into the equation results in

$$\mathcal{H}\mathbf{A} = \omega^2\mathbf{M}\mathbf{A}. \tag{61}$$

In order to remove the dependence on the mass matrix on the right side, one can rearrange the equation as

$$(\mathbf{M}^{-1/2}\mathcal{H}\mathbf{M}^{-1/2})(\mathbf{M}^{1/2}\mathbf{A}) = \omega^2(\mathbf{M}^{1/2}\mathbf{A}), \tag{62}$$

and denoting the new quantities with new symbols we have

$$\mathcal{H}'\mathbf{A}' = \alpha\mathbf{A}'. \tag{63}$$

Here, $\mathcal{H}'=\mathbf{M}^{-1/2}\mathcal{H}\mathbf{M}^{-1/2}$ is the mass-weighted Hessian matrix, $\mathbf{A}'=\mathbf{M}^{1/2}\mathbf{A}$ is the eigenvector of the mass-weighted Hessian matrix and needs to be unmass weighted for normal modes $\mathbf{A}=\mathbf{M}^{-1/2}\mathbf{A}'$, and $\alpha=\omega^2$.

The removal of translation and rotational modes can now be done using

$$\mathcal{T}' = \mathbf{M}^{1/2}\mathcal{T}, \tag{64}$$

$$\mathcal{R}' = \mathbf{M}^{1/2}\mathcal{R}, \tag{65}$$

where $\mathbf{c}=(1/\Sigma_i m_i)\Sigma_i^N m_i\mathbf{r}_i$ in $\mathcal{R}'$ is the center of mass of the system.[49]

We will show in this paper (case study I) that the constraints (e.g., bond, bend, dihedral, out of plane) can be properly removed by using

$$\mathbf{e}' = \mathbf{M}^{-1/2}\mathbf{e}. \tag{66}$$

The set $\mathbf{e}$ of Eq. (58) is modified with a factor $\mathbf{M}^{-1/2}$.

The mass-weighted Hessian is projected using $\mathbf{e}'$ to remove the translation, rotation, and constraints. The harmonic frequencies ν are then related to the eigenvalues of the projected and mass-weighted Hessian by

$$\nu_i = \frac{\sqrt{\alpha_i}}{2\pi}. \tag{67}$$

The normal mode i is given by $\mathbf{A}_i=\mathbf{A}_i'/\sqrt{m_i}$. The eigenvectors give the direction and relative amplitude of each atomic displacement. The value A_i/α_i is an arbitrary amplitude for displacement along normal mode i. If atoms are undergoing thermal fluctuations along each mode, the standard deviation of each atom is given by setting $A_i=\sqrt{2k_BT/m_n}$, where m_n is the atomic mass of atom n.[49,53] For the generation of the trajectory of normal mode i using N frames, the following expression applies:

$$\delta\mathbf{x}_i(t) = \sqrt{\frac{2k_BT/\mathbf{M}}{\alpha_i}}\hat{\mathbf{A}}_i\sin(2\pi t/N) \quad t=0,\ldots,N. \tag{68}$$

The magnitude of the motion depends on temperature and is inversely proportional to its frequency. The largest contribution to the atomic displacement comes from the lowest frequency normal modes, whereas for high-frequency eigenvectors, only a few atoms contribute. Note that this description breaks down for motions with zero frequency.

VI. CASE STUDY I: MODE ANALYSIS OF UNITED-ATOM *n*-BUTANE

A class of molecules that has been very successfully modeled are alkanes. There are models that use explicit hydrogens, but even the so-called united-atom description works very well for some purposes. United-atom models combine the carbon and hydrogen atoms of the methyl or methylene together into single interaction centers. A disadvantage of this grouping is that the force constants are now effective parameters and bear no real connection to, e.g., the infrared spectra. However, due to its simplicity, we have chosen n-butane to illustrate the effect of constraints on the mode analysis. The n-butane molecule is constructed from four united atoms: $CH_3-CH_2-CH_2-CH_3$. The stretch potential force constants are taken from Nath *et al.*:[54] $U_r=\frac{1}{2}k(r-r_0)^2$ with $k/k_B=96500$ K and $r_0=1.54$ Å. The bend and torsion potentials are taken from the TRAPPE force field:[55] $U_\theta=\frac{1}{2}k(\theta-\theta_0)^2$ with $k/k_B=62500$ K and $\theta_0=114°$, and $U_\phi=p_0+p_1(1+\cos\phi)+p_2(1-2\cos\phi)+p_3(1+3\cos\phi)$ with $p_0/k_B=0$ K, $p_1/k_B=355.03$ K, $p_2/k_B=-68.19$ K, and $p_3/k_B=791.32$ K. There are three bond, two bend, and one dihedral interactions.

Minimization of the n-butane molecule reveals two local minima for the dihedral at $\pm 63.4511747°$ and a global minimum at 180°. In Table I, we compare the frequencies of the minima to cases in which the dihedral angle is fixed, the dihedral and bend angles are fixed, the dihedral angle and the central bond are fixed, and the dihedral angle and all bonds are fixed, respectively. In general, the torsional modes are the lowest in frequency, and the stretch modes are the highest in frequency. Except the dihedral mode, the global minimum ($\phi=180°$) has no normal modes that change the dihedral angle (all four atoms are planar). Therefore, when the dihedral angle is kept fixed, the dihedral mode is removed, and all others remain the same. This is no longer true for the

TABLE I. Frequencies in cm^{-1} of united-atom *n*-butane in two minimum energy configurations: $\phi=180°$ (global minimum) and $\phi=63.451\,174\,7°$ (local minimum). The unconstrained *n*-butane is compared to constraint cases where the dihedral angle is fixed, the dihedral and bend angles are fixed, the dihedral angle and the central bond are fixed, and the dihedral angle and all bonds are fixed, respectively.

	Free		Fixed ϕ		Fixed ϕ, θ_1, θ_2		Fixed ϕ, r_{bc}		Fixed ϕ, r_{ab}, r_{bc}, r_{cd}	
	$\phi=180°$	$\phi=63.45°$	$\phi=180°$	$\phi=63.45°$	$\phi=180°$	$\phi=63.45°$	$\phi=180°$	$\phi=63.45°$	$\phi=180°$	$\phi=63.45°$
1	153.323	150.744								
2	288.622	296.864	288.622	227.648			324.355	248.761		
3	291.723	417.291	291.723	417.291	344.522	364.867	291.723	417.291	291.723	256.002
4	558.233	545.498	558.233	520.318	558.233	514.495	558.233	544.542	419.147	473.853
5	635.758	633.899	635.758	633.899	639.200	621.218	689.814	633.899		
6	692.391	649.398	692.391	649.385						

second local minimum where the dihedral angle movement is mixed with other movements. Constraining the dihedral changes several modes.

The frequencies here are obtained from the mass-weighted Hessian matrix, and when constraints are involved, the Hessian matrix is corrected using Eq. (66). In Fig. 4, we show the spectra of united-atom *n*-butane, analytically computed from the Hessian matrix compared to very low temperature (≈1 K) MD. The trajectories were generated in the *NVE* ensemble (constant number of particles *N*, constant volume *V*, and constant energy *E*) using a time step of 0.1 fs. The MD spectra were computed using the Fourier transform of the velocity autocorrelation function. Two cases of *n*-butane were examined: The global minimum at $\phi=180°$ and a local minimum at $\phi=63.4511747°$. The spectra of the molecule were computed using no constraints and compared to those computed by constraining the torsion angle and all three bonds (the bend angles are free). The analytical solution (Table I) matches the low temperature MD very well. Note that due to the constraints, some modes vanish, and the whole spectrum is generally affected. The case of the global minimum shows higher symmetry as indicated by the presence of some zero amplitude modes in the MD spectrum. As can be seen in Fig. 4, a slightly modified mass of one of the CH_3 groups can be used to break the symmetry, and the modes become visible (the mass modification was kept small enough to have very similar frequencies).

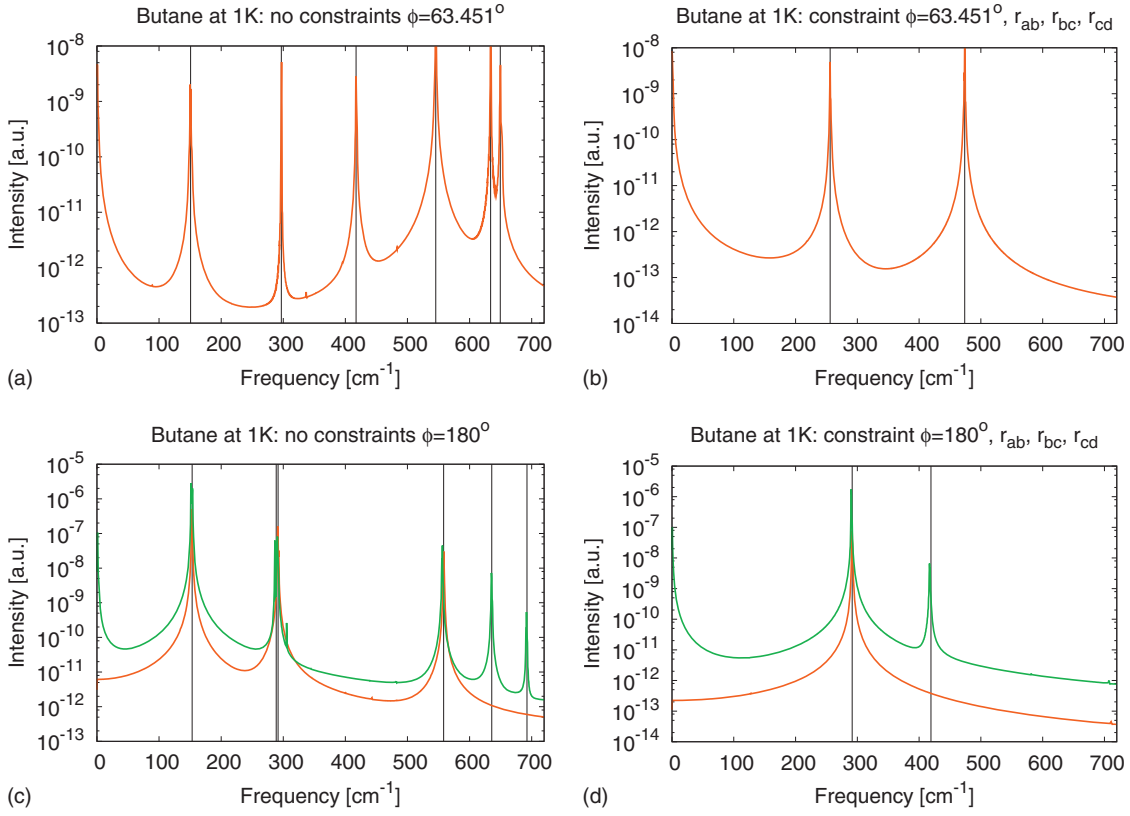

FIG. 4. Mode analysis of united-atom *n*-butane: Analytical solution compared to very low temperature (≈1 K) MD (red). Two cases are shown: A global minimum with a dihedral angle $\phi=180°$ and a local minimum at $\phi=63.4511747°$. The vertical black lines are the analytical solutions. Some amplitudes in the $\phi=180°$ case are zero due to symmetry reasons. A second spectrum (green) shows these modes by making one of the two CH_3 groups heavier by 0.5 a.u., which breaks the symmetry.

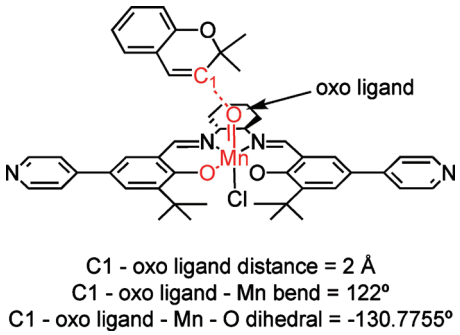

FIG. 5. The chromene-(salen)Mn complex showing the constrained distance, bend angle, and dihedral angle in red. Picture made with CHEMDRAW (Ref. 72).

VII. CASE STUDY II: MINIMIZATION OF CHROMENE APPROACH TO (SALEN)MN WITH CONSTRAINED DISTANCE, BEND ANGLE, AND DIHEDRAL ANGLE

In catalysis, insight into chirality transfer from catalyst to reactant can be gained by performing constrained minimizations of the reactant-catalyst complex. Because the mechanism of asymmetric induction for epoxidation of olefins by (salen)Mn catalysts is thought to involve steric interactions between the olefin and the catalyst, the direction of olefin approach has been studied using a combination of MM minimizations and hybrid quantum mechanics/MM calculations.[56] In the MM minimizations, the geometry was constrained to be similar to the expected transition state structure since the transition state determines the enantioselectivity of the reaction. In this work, we perform a similarly constrained minimization of a chromene-(salen)Mn complex (Fig. 5). The bond forming between the oxo ligand of the (salen)Mn and the C1 carbon of the reactant was constrained to 2.0 Å, and the bend angle defined by the Mn atom, the oxo ligand, and the C1 carbon was fixed at 122°, as done in the earlier study.[56] In previous reports,[56,57] the reactant approach dihedral angle was defined by the midpoint of the O atoms in the salen ligand, the Mn atom, the oxo ligand, and the C1 carbon. We use this definition for the approach angle except that in practice, the constrained dihedral angle uses one of the O atoms in the salen ligand instead of the midpoint of the two O atoms (see Fig. 5). The approach angle as defined in previous work can be calculated after minimization.

The generic force field DREIDING (Ref. 58) was used but modified as described in Ref. 59 to accurately model the chromene-(salen)Mn complex. To perform the constrained minimization of the chromene-(salen)Mn complex, the r^2 -SHAKE, $\cos^2\theta$ -SHAKE, and ϕ -SHAKE algorithms were employed for the distance, bend angle, and dihedral angle constraints, respectively. Figure 6 shows the energy, maximum force, number of negative eigenvalues, and the shifting parameter and lowest eigenvalue as a function of the minimization iteration. The energy decreased exponentially, reaching a plateau after approximately 200 iterations. The number of negative eigenvalues remained at 6 for most of the first 200 iterations and quickly fell to zero after that. The lack of negative eigenvalues in the final minimized structure confirmed that a true minimum had been found. While the maximum force also decreased quickly after 200 iterations, it plateaued around 1 kJ/mol Å before finally falling to meet the convergence criterion of 10^{-6} kJ/mol Å in the last 50 iteration steps. The shifting parameters γ are computed with Eq.

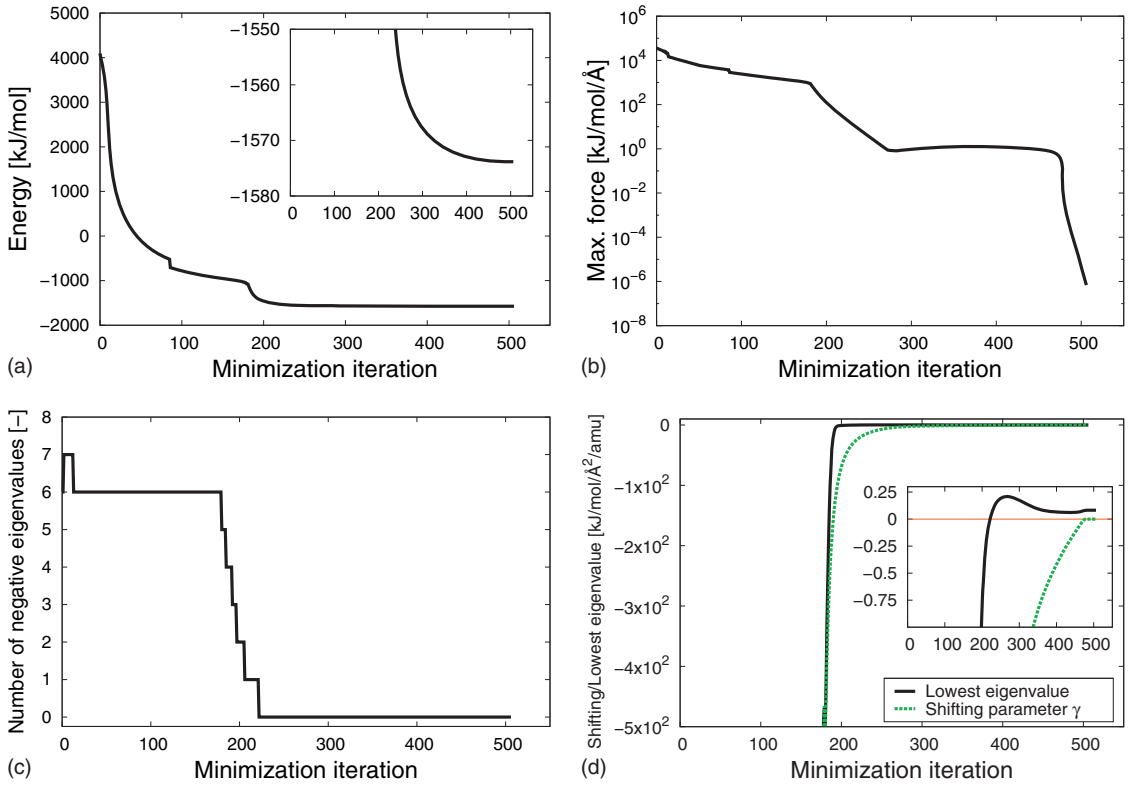

FIG. 6. Tracking the minimization process of the chromene-(salen)Mn complex: (a) The energy, (b) maximum gradient, (c) number of negative eigenvalues, and (d) the shifting parameter γ and lowest eigenvalue in the system as a function of the minimization iteration.

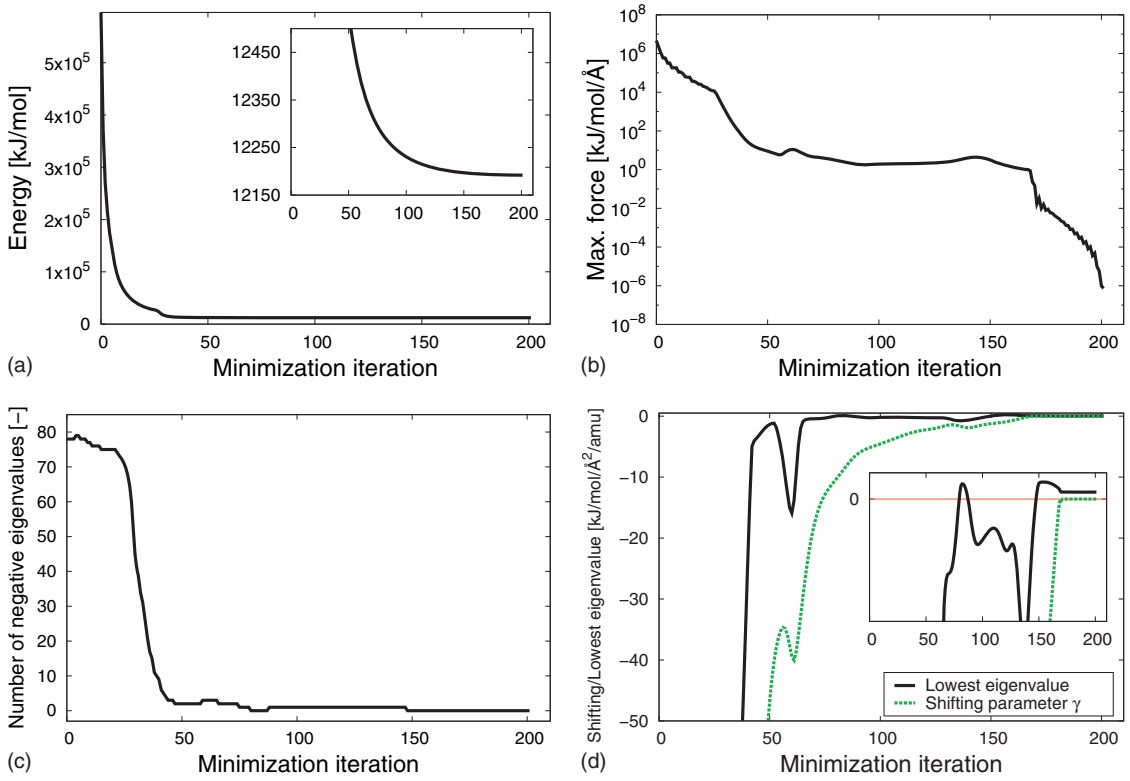

FIG. 7. Tracking the minimization process of the chromene-(salen)Mn framework: (a) The energy, (b) maximum gradient, (c) number of negative eigenvalues, and (d) the shifting parameter γ and lowest eigenvalue in the system as a function of the minimization iteration.

(53). It is the force that pushes the eigenvalues to all positive values. The shifting parameter is always lower than the lowest eigenvalue and approaches zero at convergence.[48] A movie that tracks the optimization process is provided as Supplementary Material accompanying this publication [see Ref. 30]. All movies were made with VMD (Ref. 60) as a front-end to POVRAY,[61] and mencoder[62] to convert rendered pictures to a movie.[3]

All constraints were satisfied exactly (to within a predefined tolerance): The constrained distance was 2.0 Å, the constrained angle was 122°, and the constrained dihedral was −130.7755°, translating to an approach angle of −177.59°. The modes corresponding to the constraints were removed, and this led to three zero eigenvalues for the bond, bend, and torsion constraints, respectively. These three zero eigenvalues are in addition to the six zero eigenvalues due the translation and rotation of the molecular system as a whole. During the minimization, the translational and rotational modes and constraints were removed from the Hessian matrix and the gradient.

MOFs are nanoporous, molecule-based hybrid materials built from metal nodes and organic bridging ligands. MOFs have good stability, high void volumes, and well-defined tailorable cavities of uniform size.[63–70] The recent microporous MOF compound 1 that features chiral (salen)Mn struts is highly effective as an asymmetric catalyst for olefin epoxidation.[71] The enantiomeric excess rivals that of the free molecular analog, and the framework confinement enhances catalyst stability, imparts substrate size selectivity, and permits catalyst separation and reuse. The unit cell of framework 1 has edge lengths of $a=15.1376$ Å, $b=15.2092$ Å, and $c=26.3$ Å, and cell angles $\alpha=73.271°$, $\beta=77.508°$, and $\gamma=82.596°$. A single unit cell contains 284 atoms. We used a $2\times2\times2$ system with periodic boundary conditions. The charge-charge interaction was computed using the Ewald summation (relative precision $10^{-8}\rightarrow\alpha=0.261417$, $\mathbf{k}=\{10,10,17\}$). To perform the constrained minimization of the chromene in 1, the r^2 -SHAKE, $\cos^2\theta$ -SHAKE, and ϕ -SHAKE algorithms were employed for the distance, bend angle, and dihedral angle constraints, respectively. The framework was kept fixed except for the chromene and two salen struts (the structure is catenated). These two struts comprise 177 framework atoms. The fixed atoms take no part in the Hessian matrix and gradient vector. They simply act as an external field. Here, there are three zero eigenvalues corresponding to the bond, bend, and torsion constraints, respectively. There are no additional zero eigenvalues because the framework is kept fixed.

Figure 7 shows the details of the minimization procedure. The energy rapidly approaches a plateau value while the forces are still around 1 kJ/mol Å. It takes additional iterations to bring the maximum force to the desired stopping criterion of 10^{-6} kJ/mol Å. Initially, the number of negative eigenvalues is much higher than for the free molecular case. This is due to the much more jagged and complicated energy landscape. The shifting values are shown in comparison to the lowest eigenvalue. This lowest eigenvalue is usually negative, and the shifting value is always lower than that value but approaches zero at convergence. By that time, the lowest eigenvalue has been changed to a positive value, and a true minimum is reached. A movie that tracks the optimi-

zation process of the chromene in 1 is provided as Supplementary Material accompanying this publication [see Ref. 30].

From Figs. 6 and 7, the following picture emerges. First, the energy can usually be lowered dramatically starting from an initial configuration. The number of negative eigenvalues remains substantial. After the energy has been lowered sufficiently, the process of negative eigenvalue removal really starts. In this region, the energy and forces can be lowered, but also an increase is possible. The largest negative eigenvalue is closer to zero, and this domain is characterized by large structural changes (a small eigenvalue/frequency means a large displacement). When all negative eigenvalues have been pushed toward positive eigenvalues, the algorithm behaves like Newton–Raphson, i.e., a fast decrease in the forces and rapid convergence.

The higher the confinement, the more difficult the minimization becomes. In fact, the minimization in 1 fails when soft constraints are used with very high force constants. However, for lower values of the force constants, the constraints are significantly violated. In contrast, the presented algorithm using hard constraints by mode-following minimization and projection of the Hessian matrix and gradients is very stable.

VIII. CONCLUSIONS

This paper presents a reliable and stable algorithm to minimize complex systems with hard constraints. The minimization algorithm is the mode-following minimization using the projector mechanism. The constraint modes, and optionally the translational and rotational modes, are removed from the Hessian and gradient. The feasibility of the constraints is restored after each step using the SHAKE methodology. We have derived the necessary SHAKE expressions for dihedral and out-of-plane angles. For mode analysis, the constraints need to be projected from the Hessian matrix while taking the mass-weighting into account. We showed how to modify the mass-weighted Hessian for bond, bend, dihedral, and out-of-plane constraints. The analytical mode analysis of united-atom *n*-butane was compared to very low temperature MD and found to be in excellent agreement. We applied the minimization algorithm on two real world examples: (a) The minimization of chromene at a fixed distance, bend angle, and dihedral angle toward a (salen)Mn catalyst, and (b) the minimization of chromene at a fixed distance, bend angle, and dihedral angle toward a (salen)Mn strut in a periodic framework. Minimization in strong confinement is a difficult problem, but the described minimization algorithm remained very reliable in contrast to using soft constraints.

ACKNOWLEDGMENTS

This work is supported by a TOP grant from the Netherlands Foundation for Fundamental Research (NWO-CW) awarded to R.K., the National Science Foundation (Grant No. CTS-0507013), and the National Defense Science and Engineering Graduate Fellowship Program (GAEO). We thank Aimee Bailey for helpful discussions and comments on the manuscript.

[1] H. Goldstein, *Classical Mechanics* (Addison-Wesley, Cambridge, 1950).
[2] D. Chakrabarti and D. J. Wales, Phys. Chem. Chem. Phys. **11**, 1970 (2009).
[3] D. Dubbeldam, R. Krishna, and R. Q. Snurr, J. Phys. Chem. C **113**, 19317 (2009).
[4] M. Mazars, J. Phys. A: Math. Theor. **40**, 1747 (2007).
[5] M. P. Allen and D. J. Tildesley, *Computer Simulation of Liquids* (Clarendon, Oxford, 1987).
[6] D. Frenkel and B. Smit, *Understanding Molecular Simulation*, 2nd ed. (Academic, London, 2002).
[7] A. Leach, *Molecular Modelling: Principles and Applications*, 2nd ed. (Prentice-Hall, Englewood Cliffs, NJ, 2001).
[8] D. C. Rapaport, *The Art of Molecular Dynamics Simulation* (Cambridge University Press, Cambridge, 1995).
[9] J.-P. Ryckaert, G. Ciccotti, and H. J. C. Berendsen, J. Comput. Phys. **23**, 327 (1977).
[10] H. C. Andersen, J. Comput. Phys. **52**, 24 (1983).
[11] P. Gonnet, J. H. Walther, and P. Koumoutsakos, Comput. Phys. Commun. **180**, 360 (2009).
[12] D.-H. Lu and D. G. Truhlar, J. Chem. Phys. **99**, 2723 (1993).
[13] J. Brokaw, K. Haas, and J. Chu, J. Chem. Theory Comput. **5**, 2050 (2009).
[14] D.-H. Lu, M. Zhao, and D. G. Truhlar, J. Comput. Chem. **12**, 376 (1991).
[15] P. H. M. Budzelaar, J. Comput. Chem. **28**, 2226 (2007).
[16] J.-P. Ryckaert, G. Arialdi, and S. Melchionna, Mol. Phys. **99**, 155 (2001).
[17] S. Miyamoto and P. A. Kollman, J. Comput. Chem. **13**, 952 (1992).
[18] Y. Duan, S. Kumar, J. M. Rosenberg, and P. A. Kollman, J. Comput. Chem. **16**, 1351 (1995).
[19] J. T. Slusher and P. T. Cummings, Mol. Simul. **18**, 213 (1996).
[20] B. Hess, H. Bekker, H. J. C. Berendsen, and J. G. E. M. Fraaije, J. Comput. Chem. **18**, 1463 (1997).
[21] T. R. Forester and W. Smith, J. Comput. Chem. **19**, 102 (1998).
[22] R. Kutteh, Comput. Phys. Commun. **119**, 159 (1999).
[23] M. Yoneya, J. Comput. Phys. **172**, 188 (2001).
[24] V. Krautler, W. F. van Gunsteren, and P. H. Hunenberger, J. Comput. Chem. **22**, 501 (2001).
[25] S. H. Lee, K. Palmo, and S. Krimm, J. Comput. Phys. **210**, 171 (2005).
[26] P. Gonnet, J. Comput. Phys. **220**, 740 (2007).
[27] B. Hess, J. Chem. Theory Comput. **4**, 116 (2008).
[28] A. G. Bailey, C. P. Lowe, and A. P. Sutton, J. Comput. Phys. **227**, 8949 (2008).
[29] A. G. Bailey and C. P. Lowe, J. Comput. Chem. **30**, 2485 (2009).
[30] See supplementary material at http://dx.doi.org/10.1063/1.3429610 for further details on SHAKE and RATTLE algorithms, for a multimedia movie that tracks the optimization process of the chromene-(salen)Mn complex (side view), and for a multimedia movie that tracks the optimization process of the chromene-(salen)Mn complex (top view), and for a multimedia movie that s the optimization process of the chromene-(salen)Mn framework.
[31] E. B. Wilson, Jr., J. D. Decious, and P. C. Cross, *Molecular Vibrations* (McGraw-Hill, New York, 1955).
[32] J.-P. Ryckaert, Mol. Phys. **55**, 549 (1985).
[33] R. Kutteh and T. P. Straatsma, in *Reviews in Computational Chemistry*, edited by K. B. Lipkowitz and D. B. Boyd (Wiley-VCH, New York, 1998), Vol. 12, pp. 75–136.
[34] B. J. Leimkuhler and R. D. Skeel, J. Comput. Phys. **112**, 117 (1994).
[35] B. J. Palmer, J. Comput. Phys. **104**, 470 (1993).
[36] J. Baker and W. Hehre, J. Comput. Chem. **12**, 606 (1991).
[37] P. Pulay, J. Comput. Chem. **3**, 556 (1982).
[38] J. Baker, J. Comput. Chem. **18**, 1079 (1997).
[39] J. Baker, J. Comput. Chem. **13**, 240 (1992).
[40] J. Baker and D. Bergeron, J. Comput. Chem. **14**, 1339 (1993).
[41] H. Taylor and J. Simons, J. Phys. Chem. **89**, 684 (1985).
[42] J. Baker, J. Comput. Chem. **14**, 1085 (1993).
[43] F. Eckert, P. Pulay, and H. Werner, J. Comput. Chem. **18**, 1473 (1997).
[44] K. Kudin, G. Scuseria, and H. Schlegel, J. Chem. Phys. **114**, 2919 (2001).
[45] J. Andzelm, R. King-Smith, and G. Fitzgerald, Chem. Phys. Lett. **335**, 321 (2001).
[46] T. Bucko, J. Hafner, and J. Angyan, J. Chem. Phys. **122**, 124508 (2005).
[47] G. Williams, J. Dugan, and R. Altman, J. Comput. Biol. **8**, 523 (2001).
[48] J. Baker, J. Comput. Chem. **7**, 385 (1986).
[49] M. J. Field, *A Practical Introduction to the Simulation of Molecular Systems* (Cambridge University Press, New York, 2007).

[50] C. J. Cerjan and W. H. Miller, J. Chem. Phys. **75**, 2800 (1981).
[51] J. Simons, P. Jorgensen, H. Taylor, and J. Ozment, J. Phys. Chem. **87**, 2745 (1983).
[52] J. del Campo and A. Koster, Croat. Chem. Acta **82**, 283 (2009).
[53] B. R. Brooks, D. Janezic, and M. Karplus, J. Comput. Chem. **16**, 1522 (1995).
[54] S. K. Nath, F. A. Escobedo, and J. J. de Pablo, J. Chem. Phys. **108**, 9905 (1998).
[55] M. G. Martin and J. I. Siepmann, J. Phys. Chem. B **102**, 2569 (1998).
[56] H. Jacobsen and L. Cavallo, Chem.-Eur. J. **7**, 800 (2001).
[57] K. N. Houk, N. C. De Mello, K. Condroski, J. Fennen, and T. Kasuga, *Echet96—Electronic Conference on Heterocyclic Chemistry* (The Royal Society of Chemistry, London, 1996) http://www.ch.ic.ac.uk/ectoc/echet96/.
[58] S. L. Mayo, B. D. Olafson, and W. A. Goddard, J. Phys. Chem. **94**, 8897 (1990).
[59] G. A. E. Oxford, R. Q. Snurr, and L. J. Broadbelt, "Hybrid quantum mechanics/molecular mechanics investigation of (salen)Mn for use in metal-organic frameworks," Ind. Eng. Chem. Res. (in press).
[60] W. Humphrey, A. Dalke, and K. Schulten, J. Mol. Graph. **14**, 33 (1996).
[61] Persistence of Vision Pty, Ltd. (2004). Persistence of Vision (TM) Raytracer. Persistence of Vision Pty. Ltd., Williamstown, Victoria, Australia. http://www.povray.org/.
[62] http://www.mplayerhq.hu.
[63] H. Li, M. Eddaoudi, M. O'Keeffe, and O. M. Yaghi, Nature (London) **402**, 276 (1999).
[64] M. Eddaoudi, J. Kim, N. Rosi, D. Vodak, J. Wachter, M. O'Keefe, and O. M. Yaghi, Science **295**, 469 (2002).
[65] O. M. Yaghi, M. O'Keeffe, N. W. Ockwig, H. K. Chae, M. Eddaoudi, and J. Kim, Nature (London) **423**, 705 (2003).
[66] S. Kitagawa, R. Kitaura, and S.-I. Noro, Angew. Chem., Int. Ed. **43**, 2334 (2004).
[67] J. L. C. Rowsell and O. M. Yaghi, Microporous Mesoporous Mater. **73**, 3 (2004).
[68] R. Q. Snurr, J. T. Hupp, and S. T. Nguyen, AIChE J. **50**, 1090 (2004).
[69] U. Mueller, M. Schubert, F. Teich, H. Puetter, K. Schierle-Arndt, and J. Pastre, J. Mater. Chem. **16**, 626 (2006).
[70] G. Férey, Chem. Soc. Rev. **37**, 191 (2007).
[71] S.-H. Cho, B. Q. Ma, S. T. Nguyen, J. T. Hupp, and T. E. Albrecht-Schmidt, Chem. Commun. (Cambridge) **2006**, 2563.
[72] N. Mills, J. Am. Chem. Soc. **128**, 13649 (2006).